1

Basics of Nanocrystals

1.1 Introduction

Nanoparticles constitute a major class of nanomaterials. Nanoparticles are zero-dimensional, possessing nanometric dimensions in all the three dimensions. The diameters of nanoparticles can vary anywhere between one and a few hundreds of nanometers. Small nanoparticles with diameters of a few nanometers are comparable to molecules. Accordingly, the electronic and atomic structures of such small nanoparticles have unusual features, markedly different from those of the bulk materials. Large nanoparticles (>20–50 nm), on the other hand, would have properties similar to those of the bulk [1]. The change in a material property as a function of size is shown schematically in Fig. 1.1. At small sizes, the properties vary irregularly and are specific to each size. At larger sizes, dependence on size is smooth and scaling laws can be derived to describe the variation in this regime. The size-dependent properties of nanoparticles include electronic, optical, magnetic, and chemical characteristics. Nanoparticles can be amorphous or crystalline. Being small in size, crystalline nanoparticles can be of single domain. Nanoparticles of metals, chalcogenides, nitrides, and oxides are often single crystalline. Crystalline nanoparticles are referred to as nanocrystals.

Nanoparticles are not new and their history can be traced back to the Roman period. Colloidal metals were used to dye glass articles and fabrics and as a therapeutic aid in the treatment of arthritis. The Purple of Cassius, formed on reacting stannic acid with chloroauric acid, was a popular purple dye in the olden days. It is actually made up of tin oxide and Au nanocrystals [2]. The Romans were adept at impregnating glass with metal particles to achieve dramatic color effects. The Lycurgus cup, a glass cup of 4th century AD, appears red in transmitted light and green in reflected light. This effect, which can be seen in the cup preserved in the British museum in London, is due to Au and Ag nanocrystals present in the walls of the cup. Maya blue, a blue dye employed by the Mayas around 7th century AD has been shown recently to consist of metal and oxide nanocrystals in addition to indigo and silica [3].

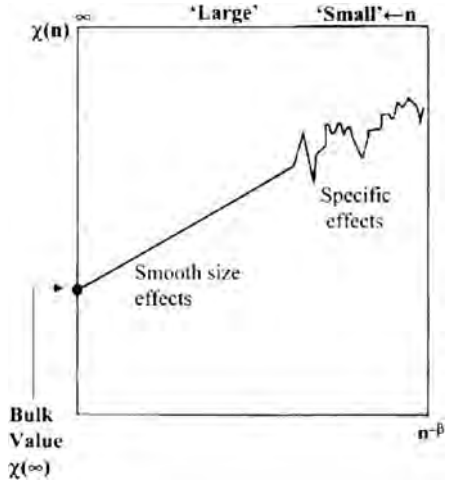

Fig. 1.1. The size dependence of a property $\chi(n)$ on the number of atoms (n) in a nanoparticle. The data are plotted against $n^{-\beta}$ where $\beta \geq 0$. Small nanoparticles reveal specific size effects, while larger particles are expected to exhibit a smooth size dependence, converging to the bulk value (reproduced with permission from [1])

Clearly, the ability to synthesize nanoparticles preceded the understanding of nanoscale phenomena. Systematic studies of nanoparticles began to appear as early as the seventeenth century. Antonio Neri, a Florentine glass maker and priest, describes the synthesis of colloidal gold in his 1612 treatise *L'Arte Vetraria*. John Kunckel, revised and translated Neri's work into german in 1689. Kunckel is often credited with the discovery that glass can be colored red by addition of gold.

Despite the early advances, studies of nanoscale particles did not gather momentum in later years. Thus, for most part of the 20th century, colloid science was the domain of a few specialized groups and did not receive sufficient importance. As early as 1857, Michael Faraday [4] carried out ground-breaking work on colloidal metals. He called them divided metals. Faraday established the very basis for the area, noting that colloidal metal sols were thermodynamically unstable, and that the individual particles must be stabilized kinetically against aggregation. Note that sols are dispersions of solids in liquids. Once the particles in a sol coagulate, the process cannot be reversed. Remarkably, Faraday also identified the essence of the nature of colloidal, nanoscale particles of metals. In the case of gold, he stated "gold is reduced in exceedingly fine particles which becoming diffused, produce a beautiful fluid ... the various preparations of gold whether ruby, green, violet, or blue ... consist of that substance in a metallic divided state." Einstein [5] related the Brownian motion executed by the nanoparticles to their diffusion coefficient. Mie and Gans [6–8] proposed a theoretical basis for the optical properties of the nanoscale particles, which continues to be used widely to this day. Frölich and Kubo proposed

theories that predicted that the electronic structure of colloidal metals would differ from bulk.

The neglect of colloid science prompted Ostwald [9] to title his 1915 book on colloids as "The world of neglected dimensions." This period also witnessed advances in methods to make colloidal gold. Bredig [10] prepared Au sols by striking an arc between Au electrodes immersed in dilute alkali. Donau [11] suggested that passing CO through a solution of chloroauric acid provided a gold sol. Zsigmondy [12] discovered the seeding method and was familiar with the use of formaldehyde in mild alkali to produce Au sols from salts. The 1925 award of the Nobel prize to Zsigmondy partly for his work on gold colloids did not seem to have enthused the scientific community to pursue this area of research. In the last few years, however, there has been a great upsurge in the use of colloid chemical methods to generate nanoparticles of various materials. This is because of the excitement caused by the science of nanomaterials initiated by the now famous lecture of Feynman [13].

Explosion of research in nanocrystals has been so dramatic that very few of the modern practitioners seem to be aware of the glorious past of colloid science. The progress has been facilitated in part by the advances in instrumentation that have helped in fully characterizing nanomaterials. Today, it is possible to prepare and study nanocrystals of metals, semiconductors and other substances by various means. Advances in both experimental and theoretical methods have led to an understanding of the properties of nanocrystals.

1.2 Properties of Nanocrystals

Nanocrystals of materials are generally obtainable as sols. Sols containing nanocrystals behave like the classical colloids. For example, the stability of a dispersion depends on the ionic strength of the medium. Nanocrystalline sols possess exceptional optical clarity. A key factor that lends stability to nanocrystal sols is the presence of a ligand shell, a layer of molecular species adsorbed on the surface of the particles. Without the ligand shell, the particles tend to aggregate to form bulk species that flocculate or settle down in the medium. Depending on the dispersion medium, the ligands lend stability to particles in two different ways. Thus, in an aqueous medium, coulomb interactions between charged ligand species provide a repulsive force to counter the attractive van der Waals force between the tiny grains, by forming an electrical double layer. In an organic medium, the loss of conformational freedom of the ligands and the apparent increase in solute concentration provide the necessary repulsive force. We illustrate this schematically in Fig. 1.2. Nanocrystals dispersed in liquids are either charge-stabilized or sterically stabilized.

Nanoparticles devoid of ligands are generally studied in vacuum. Such particles deposited on a substrate are readily examined by photoelectron spectroscopy and other techniques. Beams of uniformly sized clusters traversing

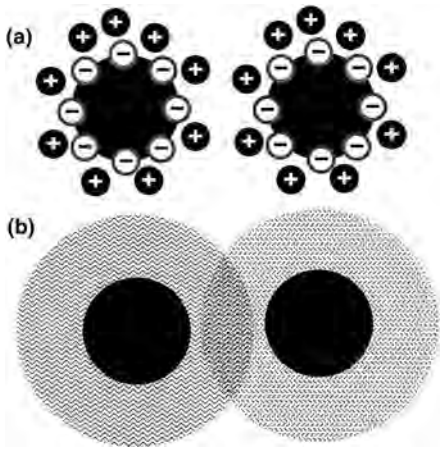

Fig. 1.2. Schematic illustration of the factors lending stability to a colloidal dispersion: (**a**) an electric double layer and (**b**) loss of conformational freedom of chain-like ligands

a vacuum chamber (cluster beams) with some fixed velocity provide opportunities for studies of the intrinsic physical properties of nanoparticulate matter.

1.2.1 Geometric Structure

The dimensions of nanocrystals are so close to atomic dimensions that an unusually high fraction of the total atoms would be present on their surfaces. For example, a particle consisting of 13 atoms, would have 12 atoms on the surface, regardless of the packing scheme followed. Such a particle has a surface more populated than the bulk. It is possible to estimate the fraction of atoms on the surface of the particle (P_s, percentage) using the simple relation,

$$P_s = 4N^{-1/3} \times 100, \tag{1.1}$$

where N is the total number of atoms in the particle [14]. The variation of the surface fraction of atoms with the number of atoms is shown in Fig. 1.3. We see that the fraction of surface atoms becomes less than 1% only when the total number of atoms is of the order of 10^7, which for a typical metal would correspond to a particle diameter of 150 nm.

Nanoparticles are generally assumed to be spherical. However, an interesting interplay exists between the morphology and the packing arrangement, specially in small nanocrystals. If one were to assume that the nanocrystals strictly follow the bulk crystalline order, the most stable structure is arrived at by simply constraining the number of surface atoms. It is reasonable to assume that the overall polyhedral shape has some of the symmetry elements of the constituent lattice. Polyhedra such as the tetrahedron, the octahedron,

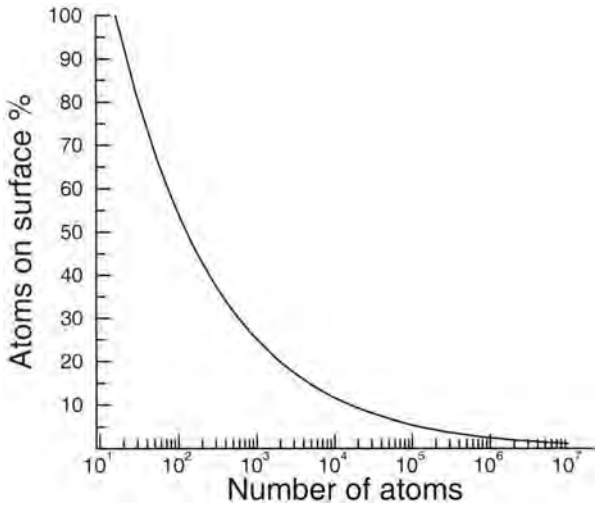

Fig. 1.3. Plot of the number of atoms vs. the percentage of atoms located on the surface of a particle. The calculation of the percentage of atoms is made on the basis of (1.1) and is valid for metal particles

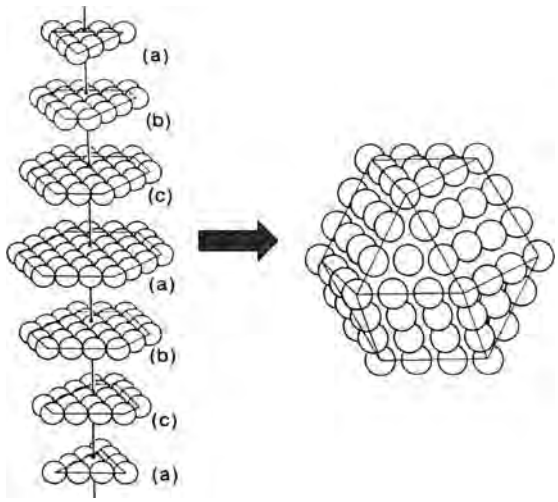

Fig. 1.4. Schematic illustration of how a cuboctahedral 147 atom-cluster, composed of seven close-packed layers can be made out of a stacking sequence reminiscent of a fcc lattice (reproduced with permission from [16])

and the cuboctahedron can be constructed following the packing scheme of a fcc lattice [15, 16]. Figure 1.4 shows how a cuboctahedral cluster of 146 constituent atoms follows from a fcc type *abcabc* layer stacking. In contrast to the above, small clusters frequently adopt *non-close packed* icosahedral

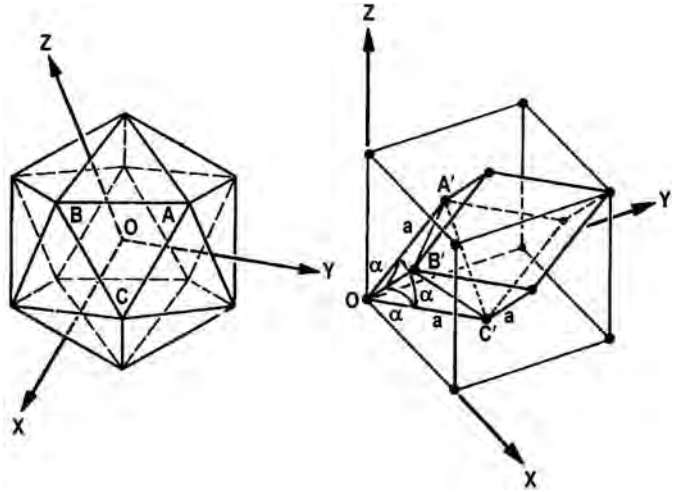

Fig. 1.5. The regular icosahedron is made up of twenty irregular tetrahedra like OABX. The rhombhohedral cell in a fcc lattice (OA′B′C′) has $\alpha = 60°$. When α is distorted to 63.43°, OA′B′C′ and OABC become similar. Small nanocrystals distort in a similar manner from regular fcc lattice to adopt the icosahedral shape

or dodecahedral shapes. The clusters adopting such schemes suffer a loss in packing efficiency. The icosahedron has a fivefold symmetry, inconsistent with the packing requirements of a regular crystalline lattice with long-range order. While employing close packing schemes, a stacking fault becomes necessary to arrive at an icosahedral arrangement. Such a scheme is outlined in Fig. 1.5.

The icosahedron which has twenty triangular faces and twelve vertices consists of a fcc-like close packing. Each of the twenty triangular faces of an icosahedron can be considered as a base of a tetrahedron, whose apex is at the inversion center (see Fig. 1.5a). A tetrahedron OA′B′C′ in Fig. 1.5b joining three face-centered atoms and an atom at the base of a fcc unit cell has the angle, $\alpha = 60°$. These angles can be distorted to 63.43°, to obtain the tetrahedron (OABC) that forms the building block of an icosahedron. Such a distortion results in the lowering of the packing fraction from 0.74080 to 0.68818. Several theoretical investigations have sought to explain the unusual stability of icosahedral clusters [17–19]. Allpress and Sanders [20, 21], based on potential energy calculations, showed that the binding energy per atom is lower than that in a corresponding octahedron containing the same number of atoms. Molecular dynamics simulations have shown that Al clusters with nuclearities upto 147 atoms exhibit distorted icosahedral structures while Al_{147} has a cuboctahedral shape [22]. More rigourous theories (ab initio, density functional) broadly support this contention. A decahedral shape can be thought of as being made up of four edge-sharing tetrahedra, followed by some relaxation and the consequent loss of packing fraction. Ino [23, 24]

has suggested the use of the term "multiply twinned particle" to denote a decahedral particle, and such particles obtained by the twining of tetrahedra.

The properties of nanocrystals are also influenced by the formation of geometric shells which occur at definite nuclearities [25, 26]. Such nuclearities, called magic nuclearities endow a special stability to nanocrystals as can be demonstrated on the basis of purely geometric arguments. A new shell of a particle emerges when the coordination sphere of an inner central atom or shell (forming the previous shell) is completely satisfied. The number of atoms or spheres required to complete successive coordination shells is a problem that mathematicians, starting with Kepler, have grappled with for a long time [27, 28]. The "kissing" problem, as it is known in the mathematical world, was the subject of a famous argument between Newton and Gregory at Cambridge. In retrospect, Newton, who held that 12 atoms are required to complete the second shell was indeed correct. An idea of the mathematical effort involved can be gauged from the fact that the proof of Newton's argument was provided only in 2002. It is quite apparent that the ultimate shape of the emerging crystallite should play a role in determining the number of atoms that go into forming complete shells. The magic nuclearities would then yield information on the morphology of the cluster. By a strange coincidence, the number of atoms required to form complete shells in the two most common shapes (icosahedron and cuboctahderon) is the same.

The number of atoms, N, required to form a cluster with L geometric shells is given by

$$N = \frac{(10L^3 + 15L^2 + 11L + 3)}{3}. \tag{1.2}$$

This represents the solution for the "kissing" problem in three dimensions and is valid for icosahedral and cuboctahedral morphologies. For other shapes, the reader may refer to a paper from the group of Martin [29]. Particles possessing the above number of atoms are said to be in a closed-shell configuration. The number of atoms required to fill up coordination shell completely, n_L of a particular shell, is given by

$$n_L = (10n_{L-1}^2 + 2). \tag{1.3}$$

where n_0=1. Thus, 12 atoms are required to complete the first shell, 42 to complete the second shell etc. A schematic illustration of the observed magic nuclearity clusters is provided in Fig. 1.6. The notion of the closed-shell configuration can be extended to larger dimensions as well. Closed-shell configurations lend stability to giant clusters made of clusters and even to a cluster of giant clusters.

Determination of the structures of nanocrystals should ideally follow from X-ray diffraction, but small particles do not diffract well owing to their limited size. The peaks in the diffraction pattern are less intense and are broad. Structural studies are therefore based on high resolution transmission electron microscopy (HRTEM), extended X-ray absorbtion fine structure (EXAFS),

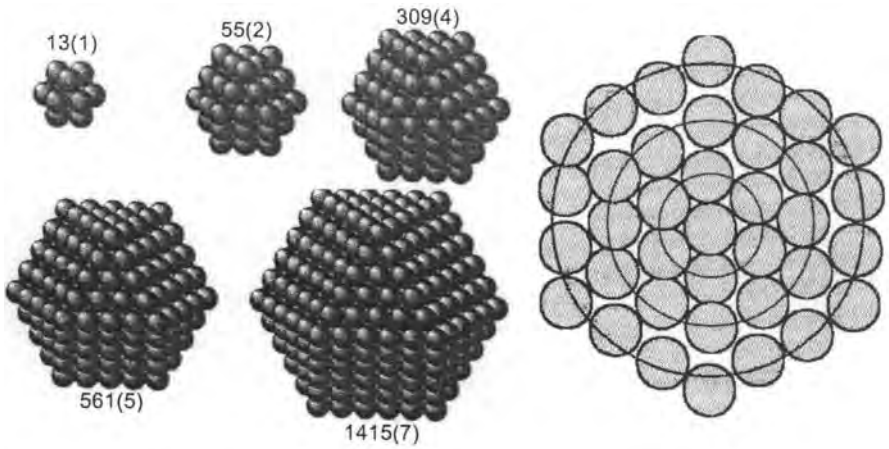

Fig. 1.6. Nanocrystals in closed-shell configurations with magic number of atoms. The numbers beside correspond to the nuclearity (N) and the number of shells (L). The figure on the left is a cross-sectional view showing five coordination shells in a 561 atom cluster

scanning tunneling microscopy (STM) and atomic force microscopy (AFM). X-ray diffraction patterns provide estimates of the diameters (D) of nanocrystals from the width of the diffraction profiles, by the use of the Scherrer formula [30]

$$D = \frac{0.9\lambda}{\beta \cos\theta}. \tag{1.4}$$

Here, β is the full-width at half-maximum of the broadened X-ray peak corrected for the instrumental width,

$$\beta = \beta^2_{\text{observed}} - \beta^2_{\text{instrumental}}. \tag{1.5}$$

Estimates based on the Scherrer relation are used routinely. It is desirable to carry out a Reitveld analysis of the broad profiles of nanoparticles to obtain estimates of D.

HRTEM with its ability to image atomic distributions in real space, is a popular and powerful method. The icosahedral structure of nanocrystals is directly observed by HRTEM and evidence for twinning (required to transform a crystalline arrangement to an icosahedron) is also obtained by this means (see Fig. 1.7) [15, 31]. The images are often compared with the simulated ones [32, 33]. High resolution imaging provides compelling evidence for the presence of multiply twinned crystallites specially in the case of Au and Ag nanoparticles [34]. Characterization by electron microscopy also has certain problems. For example, the ligands are stripped from the clusters under the electron beam; the beam could also induce phase transitions and other dynamic events like quasi-melting and lattice reconstruction [35]. The fact

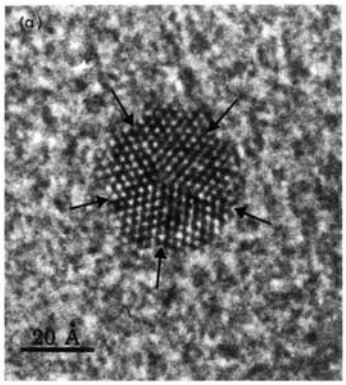

Fig. 1.7. A high resolution TEM image showing the icosahedral shape and the five fold symmetry axis of a Ag nanoparticle (reproduced with permission from [31])

that ligands desorb from clusters has made it impossible to follow the influence of the ligand shell on cluster packing.

STM, with its ability to resolve atoms, provides exciting opportunities to study the size and morphology of individual nanoparticles. In the case of ligated nanocrystals, the diameters obtained by STM include the thickness of the ligand shell [36]. Ultra high vacuum STM facilitates in situ studies of clusters deposited on a substrate. Furthermore, it is possible to manipulate individual nanoscale particles using STM. However, it is not possible to probe the internal structure of a nanocrystal, especially if it is covered with a ligand shell. AFM supplements STM and provides softer ways of imaging nanocrystals. EXAFS has advantages over the other techniques in providing an ensemble average, and is complimentary to HRTEM [37].

1.2.2 Magnetic Properties of Nanocrystals

Isolated atoms of most elements possess magnetic moments that can be arrived at on the basis of Hund's rules. In the bulk, however, only a few solids are magnetic. Nanoscale particles provide opportunities to study the evolution of magnetic properties from the atomic scale to the bulk. Even before the explosion of interest in nanoscience, magnetic properties of the so-called fine particles had been examined. In fact, size effects were perhaps first noticed in magnetic measurements on particles with diameters in the 10–100 nm range [38].

In order to understand size-dependent magnetic properties, it is instructive to follow the changes in a magnetic substance as the particle size is decreased from a few microns to a few nanometers. In a ferromagnetic substance, the T_c decreases with decrease in size. This is true of all transition temperatures associated with long-range order. For example, ferroelectric transition temperatures also decrease with particle size. With the decrease in the diameter,

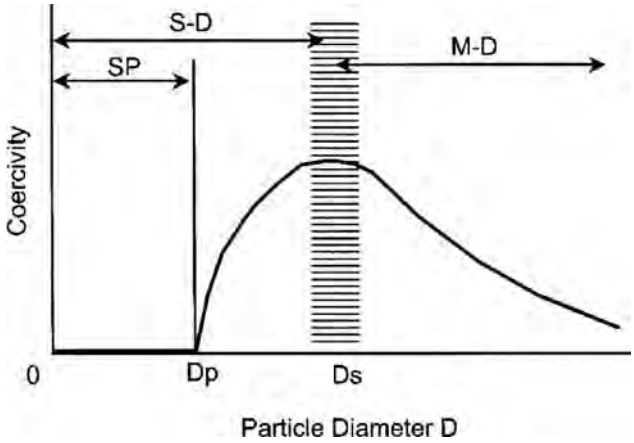

Fig. 1.8. Schematic illustration of the change in the coercivity of a ferromagnetic particle with the diameter. SP denotes the superparamagnetic regime, S-D the single-domain regime and M-D the multi-domain regime

the coercivity (H_c), increases initially till a particular diameter, D_s, and thereafter decreases as shown in Fig. 1.8. The critical diameter, D_s, marks a region wherein the particle changes from being a multi-domain particle to a single-domain particle. The value of D_s is normally a few tens of nanometers. The single-domain nature of the nanoparticle is its single most attractive magnetic property. Below D_s, H_c tends to decrease due to thermal effects and follows a relation of the form:

$$H_c = g - \frac{h}{D^{3/2}}, \tag{1.6}$$

where g and h are constants [39]. Below the critical diameter D_p, coercivity becomes zero as the thermal energy would be sufficient to randomize the magnetic moments in the particle. Nanocrystals below the diameter D_p ($\sim$10 nm), exhibit such a behavior and are said to be superparamagnetic. Superparamagnetic particles do not possess long-range magnetic order, but show characteristic magnetic properties at low temperatures [40]. Particles delineated on the basis of the above critical regimes, follow different paths to the final magnetized state and the magnetization reversal mechanism. These paths and mechanisms are rather complicated [39].

Size-dependent changes in magnetic anisotropy are another aspect of interest. A magnetic material exhibits strong and often complex anisotropic behavior when subjected to magnetization. The magnetic anisotropic energy (E), defined as the energy difference involved in changing the magnetization direction from a low-energy direction or easy axis to a high energy direction or hard axis, is an important technological parameter. Materials with high E and low E find numerous applications. The simplest form of anisotropy is the uniaxial anisotropy, where E is only dependent on the angle that the magnetic

field vector makes with the easy axis of the sample. Square hysteresis loops are obtained when the direction of magnetization is parallel to the easy axis and a straight line response is obtained when the field direction is perpendicular to the easy axis direction [41, 42]. Materials are also known to exhibit hexagonal and cubic anisotropy. The nature of magnetic anisotropy can be arrived at by studying hysteresis loops obtained along various directions. E exhibits dramatic changes with the change in size and shape. Nanoparticles generally possess higher E, but may also show a change in the basic nature of anisotropy.

Superparamagnetic behavior is caused by thermal flipping of the anisotropic barrier to magnetization reversal. Below a certain temperature, called the blocking temperature, temperature-induced flipping or relaxation can be arrested and the nanocrystals acquire a finite coercivity. In Fig. 1.9, magnetic measurements indicating size-dependent changes in the blocking temperature of $CoFe_2O_4$ nanoparticles are shown. The superparamagnetic behavior was first modeled by Neel in the 1950s [43]. In the case of nanoparticles with uniaxial anisotropy, Neel's theory suggests that the temperature induced relaxation varies exponentially with temperature and scales with the sample volume. Besides the loss of coercivity, another characteristic feature

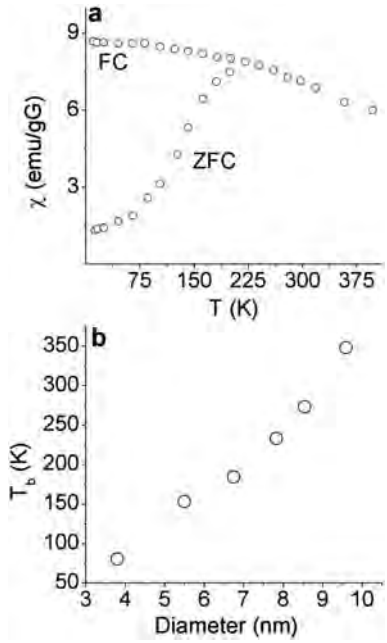

Fig. 1.9. (**a**) Magnetic susceptibility vs. temperature for $CoFe_2O_4$ nanoparticles under field cooled and zero-field cooled conditions. The applied field is 2,000 G. (**b**) shows the variation of blocking temperature (T_b) with diameter of nanoparticles (plot produced with data from [40])

of superparamagnetic behavior is the scaling of magnetization with temperature. A plot of the magnetization (M) and the ratio of the magnetic field and the temperature (H/T) produces a universal curve for all temperatures above T_b. Experimentally, superparamagnetism may be probed by techniques such as neutron scattering, Mössbauer spectroscopy and magnetization measurements. Since superparamagnetic behavior is related to the relaxation rate, it is sensitive to the characteristic time scale of measurement. In the experimental techniques indicated above, the time scales of measurements vary over a wide range (10^{-14}–10^{-12} for neutron scattering to around 10 s for magnetization measurement) and different measurements, therefore, yield different blocking temperatures. Though the scaling with volume suggested by the Neel theory is largely followed in the uniaxial cases, the actual blocking behavior of magnetic nanocrystals, especially those of the oxides are quite complicated. Effects due to the ligand shell and lattice defects are generally considered to be responsible for the observed deviations.

Many metal oxide nanoparticles are known to show evidence for the presence of ferromagnetic interactions at low temperatures. This is specially true of nanoparticles of antiferromagnetic oxides such as MnO, CoO, and NiO [44,45]. What one normally observes is a divergence in the zero-field cooled and field cooled magnetization data at low temperatures. The materials show magnetic hysteresis below a blocking temperature typical of superparamagnetic materials. The blocking temperature generally increases with the particle size. In Fig. 1.10, we show the magnetization behavior of NiO particles of 3 and 7 nm diameters [45].

While reasonable progress has been made in understanding the magnetic properties of isolated particles, ensembles of particles represent a relatively poorly researched area [46, 47]. A typical ensemble consists of particles with distributions in size, shape and easy anisotropy direction. Further, interparticle interactions play a role in determining the magnetic response of the ensemble. Theoretical investigations predict interesting phenomena in such assemblies, including changes in the mechanism of magnetization, depending on interparticle interactions. Experimentally, controlled interactions are brought about by varying parameters such as the volumetric packing density. Experiments have been carried out on ensembles of nanoparticles obtained in various ways such as freezing a sol containing a known fraction of magnetic nanoparticles or dilution in a polymer matrix [41, 46–48]. Seminal advances have been made in obtaining such ensembles by self-assembly based techniques. Self-assembled nanocrystalline ensembles posses several advantages over those obtained by other means.

1.2.3 Electronic Properties

Bulk metals possess a partially filled electronic band and their ability to conduct electrons is due to the availability of a continuum of energy levels above E_F, the fermi level. These levels can easily be populated by applying an

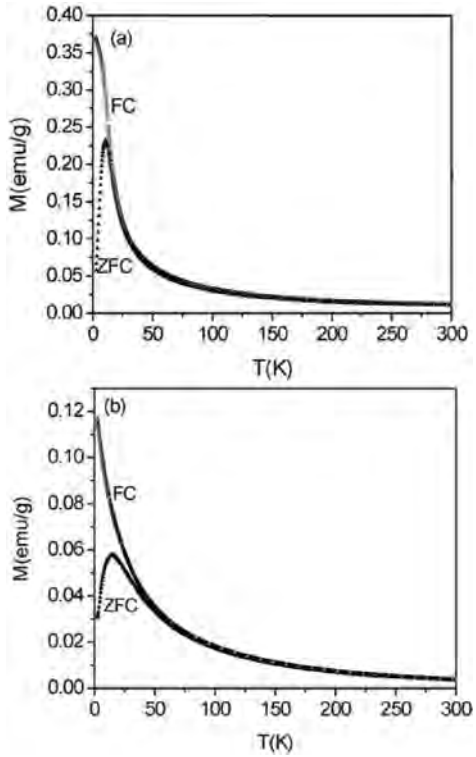

Fig. 1.10. The temperature dependence of dc magnetization of (**a**) 3 nm and (**b**) 7 nm NiO nanoparticles under zero-field cooled and field cooled conditions (H = 100 Oe)(reproduced with permission from [45])

electric field and the electrons now behave as delocalized Bloch waves ($\lambda \sim$ 5–10 Å) [14]. When a metal is divided finely, the continuum of the electronic states breaks down and the sample ultimately becomes insulating. The discreteness of energy levels do not physically manifest themselves as long as the gap is less than $k_{\mathrm{b}}T$, the thermal energy at temperature T. The discreteness of the levels can be measured in terms of average spacing between the successive quantum levels, δ, given by

$$\delta = \frac{4E_F}{3n_{\mathrm{e}}}, \tag{1.7}$$

and is known as the Kubo gap [49]. Here, n_{e} is the number of valence electrons in the cluster (a contribution of one valence electron per constituent atom is assumed). In the case of semiconductors, a reduction in the size of the system causes the energy levels at the band edge to become discrete, with interlevel spacings similar to metals. This effectively increases the bandgap of the semiconductor [50]. The issues at hand are sketched schematically in

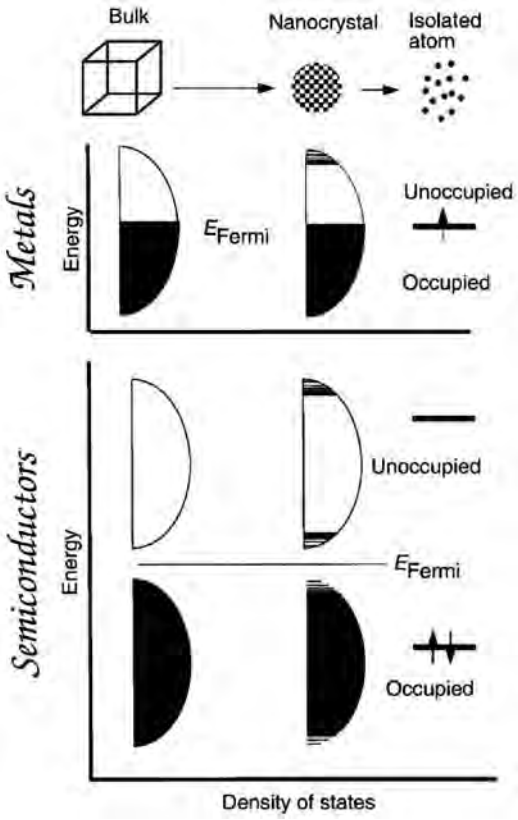

Fig. 1.11. Schematic illustration of the changes in the electronic structure accompanying a reduction in size, in metals and semiconductors

Fig. 1.11. Additional complications are introduced by the strongly directional covalent bonds present in a semiconductor. Accompanying the appearance of the discrete levels are other consequences such as the change from metallic to van der Waals type of bonding, lowering of the melting point, odd–even effects, and perhaps most significantly, a metal–insulator transition. The whole gamut of such changes are generally called as quantum size effects [51].

Another consideration required to describe the electronic structure of metal clusters is the emergence of electronic shells. The closure of electronic shells, similar to the closure of geometric shells, bequeath special stability to specific nuclearities and is manifest best in the variation of ionization energies with cluster nuclearity [29, 52]. The total number of electrons required to arrive at successive closed-shell configuration is 2, 10, 28, 60.... The closed shell configuration is based on a hydrogen atom-like potential and hence the familiar 2, 8, 18, 32 pattern for the outer electron configuration to fill the electronic shells in the clusters. Other theoretical models predict different sets of

closed-shell configurations. A unified picture of both geometric and electronic shells can be obtained by considering a characteristic length in closed-shell configurations [16,29]. A unit increase of the characteristic length scale results in the closure of a shell. For geometric clusters, the characteristic length is the interatomic distance, while the characteristic length for electronic shells is related to the electron wavelength in the highest occupied level. In the case of alkali metal clusters, this wavelength is around twice the interatomic distance.

Experimental evidence for electronic shells is found in the plot of cluster abundance vs. nuclearity and in the variation of the ionization energies of clusters (see Fig. 1.12). Electronic shell effects dominate the properties of alkali metal clusters. They are also broadly applicable to p-block metals. The properties of transition and nobel metal nanoparticles, however, are influenced more by the formation of geometric shells. In fact, a transition from shells of electrons to shells of atoms is seen in the case of Al [29, 53]. It appears that the abundance of available oxidation states and the directional nature of the d- and f-orbitals (and to a limited extent, of the p-orbital) play a role in determining the shell that governs the property of a particular cluster.

A host of physical techniques has been used to follow phenomena such as the closure of the bandgap and the emergence of the metallic state from the cluster regime. Photoelectron spectroscopy methods are among the most popular methods to study nanoparticles. Core level X-ray photoelectron spectroscopy (XPS) provides information on the oxidation state of the atoms. Changes in the electronic structure are manifested as binding energy shifts and through the broadening of photoemission bands. XPS is ideally suited to study changes in the electronic structure of clusters, accompanying the

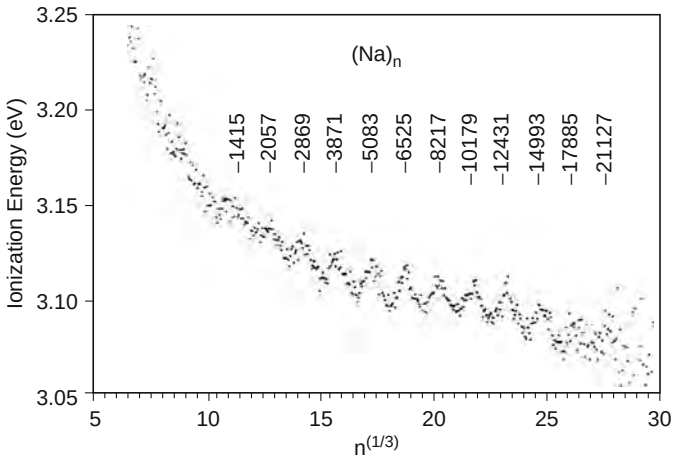

Fig. 1.12. Ionization energies of Na clusters vs. the third root of cluster nuclearity. The oscillations occur at closed shell nuclearities. The nuclearities are indicated on top (reproduced with permission from [16])

adsorption of gases. The density of states around the fermi level can be probed by means of ultraviolet photoelectron spectroscopy (UPS), while Bremsstrahlung isochromat spectroscopy (BIS) provides information on the unoccupied levels. Direct information on the gap states in nanocrystals of metals and semiconductors is obtained by scanning tunneling spectroscopy (STS). This technique provides the desired sensitivity and spatial resolution making it possible to carry out tunneling spectroscopic measurements on individual particles. The various techniques and the region of the band structure probed by them are schematically illustrated in Fig. 1.13.

Nanoscale particles of metals and semiconductors have been subject to numerous theoretical investigations [54]. Theories have evolved in sophistication and rigor since the beginnings made by Kubo and Frolich. The electronic and geometric structure of nobel metal clusters containing up to a few hundred atoms are studied using ab initio calculations. A few surprises have resulted from such investigations. For example, detailed calculations on anionic coinage metal clusters with seven atoms have indicated that while Cu_7^- and Ag_7^-

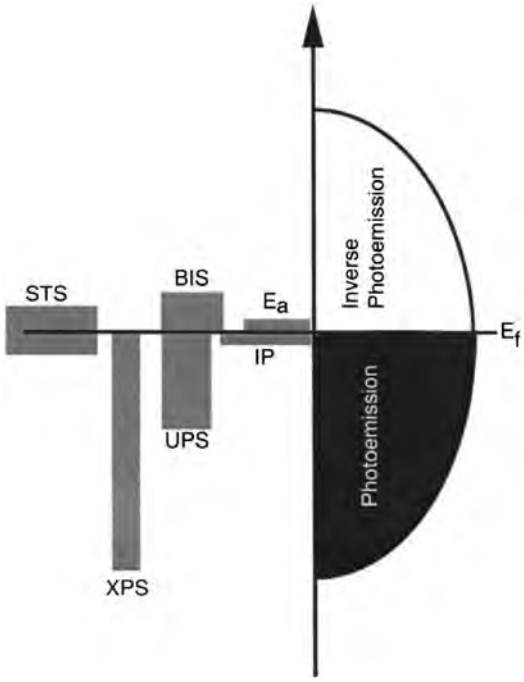

Fig. 1.13. A schematic illustration of the spectroscopic techniques and the portion of the band structure that they probe. The techniques illustrated are ionization potential (IP) measurements, electron affinity measurements (E_a), Bremsstrahlung isochromat spectroscopy (BIS), Ultraviolet photoelectron spectroscopy (UPS), X-ray photoelectron spectroscopy (XPS), Scanning tunneling spectroscopy (STS)

have three dimensional structures, Au_7^- is planar [55]. Planar structures are energetically favored for other Au nuclearities as well [56]. Ab initio molecular dynamics simulations have been carried out on clusters containing up to a few tens of atoms. For example, Landman and coworkers [57, 58] have carried out extensive computer simulations, on the structure and dynamics of alkanethiol-capped Au nanocrystals of different sizes. Numerous methods have been devised to study the properties of larger clusters often borrowing from theories used to model the bulk. Self-consistent Jellium model and local density approximation (a DFT based method) are popular for the study of metal clusters. The latter is also useful to investigate semiconductor nanocrystals. Tight-binding approximation based methods are used to study tetrahedrally coordinated semiconductors. Currently, experiments and theories go hand in hand in the study of small particles ($\sim$1 nm) and as the methods develop, it is not difficult to visualize a time in the near future, where the same can be said for investigations on larger nanocrystals.

In a bulk metal, the energies required to add or remove an electron are equivalent and are called the work function (W). In contrast, in the case of a molecule, the corresponding energies, electron affinity (E_a) and ionization potential (IP) are nonequivalent [59]. The two energies differ to a smaller extent in a nanoparticle and are size-dependent. E_a and IP are given by

$$\mathrm{IP} = W + \frac{\alpha e^2}{R} \tag{1.8}$$

$$E_\mathrm{a} = W + \frac{\beta e^2}{R} \tag{1.9}$$

with the constraint,

$$\alpha + \beta = 1 \tag{1.10}$$

Here, R is the radius of the particle and α and β are constants. The physical significance and the values of α and β have been a subject of much debate. It appears that the value $\alpha = 3/8$ is appropriate for alkali metal clusters while $\alpha = 1/2$ agrees with the experimental results on nobel metal particles [52, 60]. The difference in the two energies, E_a and IP, is the charging energy, U, given by,

$$U = \mathrm{IP} - E_\mathrm{a} = \frac{(\alpha - \beta)e^2}{R}. \tag{1.11}$$

Typical values of U are of the order of a few hundred meV. It is to be noted that U is manifest as a Coulombic gap and is different from the electronic energy gap. It is possible to define differences between successive IPs and E_as and arrive at various states called the Coulombic states, defined by successive Us. The Coulombic states are presumed to be similar for both semiconductor and metallic nanocrystals unlike the electronic states [61]. A quantity closely related to U that aids in a better understanding is the capacitance (C) of a particle, which is given by

$$C = \frac{U}{2e}. \tag{1.12}$$

The classical expression for the capacitance of a metal sphere embedded in a dielectric with a dielectric constant, ϵ_{m} is

$$C = 4\pi\epsilon\epsilon_{\mathrm{m}}R. \tag{1.13}$$

Equations 1.12 and 1.13, agree with each other and yield capacitances of the order of 10^{-18} F (or 1 aF) for nanoparticles. In this regime of finite charging energies and low capacitances, the charging of a capacitor is no longer continuous, but is discrete. For a current to flow through a nanocrystal, an external voltage V_{ext} greater than $\frac{e}{2C}$ is required. This phenomena of current exclusion across zero bias is called Coulomb blockade. When the Coulomb blockade barrier is broken applying sufficient voltage, electrons tunnel into the nanocrystal and tunnel out almost immediately. The electrons may reside long enough to provide a voltage feedback preventing an additional electron from tunneling in simultaneously. A continuous one electron current, I given by

$$I = \frac{e}{2RC} \tag{1.14}$$

flows through the circuit. To place an additional electron on the nanocrystal, a full e/C increase in voltage is required. Thus, steps called a Coulomb staircase becomes visible in the IV spectra of nanocrystals. A schematic illustration of a Coulomb staircase observed in the IV spectra is given in Fig. 1.14. While Coulomb blockade is ordinarily observed, the observation of a Coulomb staircase, requires a tuning of the circuit characteristics. The most significant impact of this discovery is in the realization of single electron

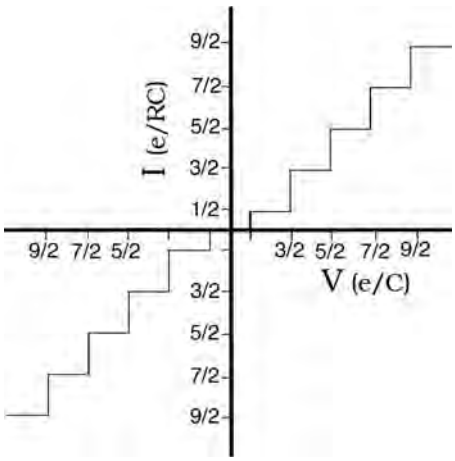

Fig. 1.14. Schematic illustration of the Coulomb staircase behavior seen in the I-V spectra

devices at room temperature [62–65]. Exploratory single electron devices, including single electron transistors, operable at room temperature have been realized by exploiting the low capacitance of nanocrystals [62–64]. Single electron devices use the smallest possible charge to store information and hence are among the most efficient of known devices. It is indeed fascinating that the measurement of IP and E_{a} has led to such possibilities.

1.2.4 Optical Properties

The electronic absorption spectra of nanocrystals of metals is dominated by the surface plasmon band which arises due to the collective coherent excitation of the free electrons within the conduction band [66–69]. A schematic illustration of the electric field component of an incoming light wave inducing a polarization of the free or itinerant electrons is shown in Fig. 1.15. It corresponds to the dipolar excitation mode which is the most relevant for particles whose diameters are much less than the wavelength of light. However, higher order excitations are possible and come into play for nanocrystals with diameters in the range of tens of nanometers.

As mentioned earlier, the theory of optical absorption of small particles was proposed by Mie in 1908 [6]. Mie's electrodynamic solution to the problem of light interacting with particles involved solving Maxwell's equations with appropriate boundary conditions and leads to a series of multipole oscillations for the extinction (C_{ext}) and scattering (C_{sca}) cross-sections of the nanoparticles. Thus

$$C_{\mathrm{ext}} = \frac{2\pi}{k^2} \sum_{n=1}^{\infty} (2n+1) Re(a_n + b_n)\,, \tag{1.15}$$

$$C_{\mathrm{sca}} = \frac{2\pi}{|k|^2} \sum_{n=1}^{\infty} (2n+1) Re(|a_n|^2 + |b_n|^2)\,, \tag{1.16}$$

Fig. 1.15. A schematic illustration of the excitation of the dipole surface plasmon oscillation by the electric field component of the light wave. The dipolar oscillation of the electrons has the same frequency as that of the incoming light wave

where ϵ_{m} is the dielectric constant of the surrounding medium, $k = \frac{2\pi\sqrt{\epsilon_{\mathrm{m}}}}{\lambda}$, a_n and b_n are Ricatti–Bessel functions that depend on the wavelength and the nanoparticle radius (R). For small particles, the scattering term and the higher order extinction terms are negligible. The extinction coefficient is, therefore, given by,

$$C_{\mathrm{ext}} = \frac{24\pi^2 R^3 \epsilon_m^{3/2}}{\lambda} \frac{\epsilon_2}{(\epsilon_1 + 2\epsilon_m)^2 + {\epsilon_2}^2}\,, \tag{1.17}$$

where ϵ_1 and ϵ_2 are the real and imaginary part of the frequency-dependent dielectric constant, ϵ, of the substance. The dielectric constants can either be obtained from the Drude free electron model or from experiments [70]. The Drude model relates the dielectric constant to the bulk plasmon frequency, ω_{p}, and the dampening frequency, ω_{d}, which are given by

$$\omega_{\mathrm{p}} = \frac{N_{\mathrm{e}} e^2}{m_{\mathrm{e}}^* \epsilon}\,, \tag{1.18}$$

$$\omega_{\mathrm{d}} = \frac{V_{\mathrm{f}}}{L}\,, \tag{1.19}$$

where N_{e} is the concentration of the free electrons, m_{e}^* the effective mass of the electron, V_{f} the velocity of the electrons at the fermi level and L, the mean free path. Small particles with diameters comparable to the mean free path exhibit a diameter dependent L, given by,

$$\frac{1}{L_{\mathrm{effective}}} = \frac{1}{2R} + \frac{1}{L}. \tag{1.20}$$

The origin of color lies in the denominator of (1.17), which predicts an absorbance maximum for a sol, when

$$\epsilon_1 = -2\epsilon_m. \tag{1.21}$$

Thus, metal nanocrystals of various sizes exhibit characteristic colors depending on their diameters and the dielectric constant of the surrounding medium. Typical size-dependent changes in the optical spectra are shown in Fig. 1.16. Mathematical methods have been developed to accurately compute the higher order terms in Mie's theory [71]. Several off-the-shelf programs are available to apply Mie's theory and its extensions to a variety of nanoparticles [72]. One such code called "BHCOAT," presented in the book by Bohren and Huffman [73] is very popular.

The somewhat complicated nature of surface plasmon excitation and its dependence on factors such as the distribution in particle diameters have thwarted attempts to derive fundamental physical quantities and to obtain quantitative information on the electronic structure of fine particles based on plasmon resonance spectroscopy. Initial studies such as those due to Kreker and Kreibig [74, 75] have been instrumental in verifying the validity of Mie's

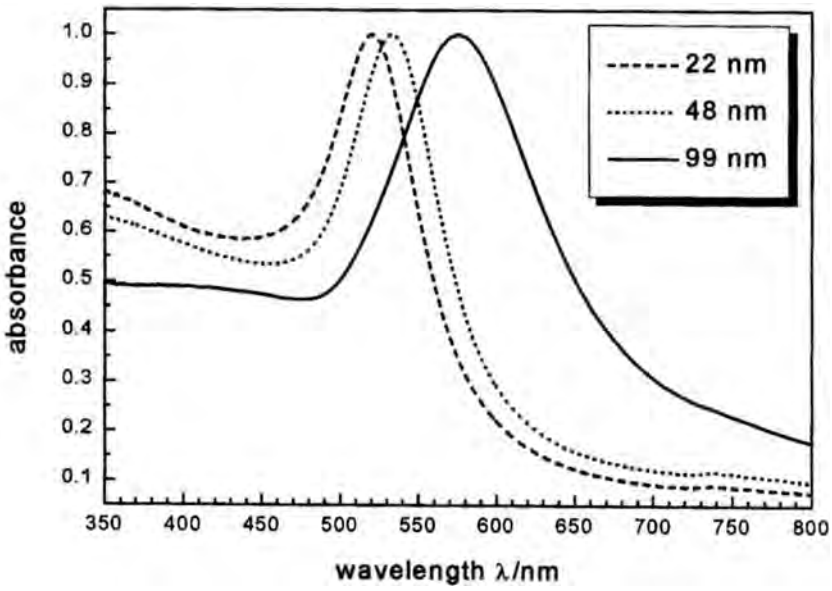

Fig. 1.16. Optical absorption spectra of gold nanoparticles with diameters of 22, 48, and 99 nm (reproduced with permission from [66])

theory for noble metal particles such as Au and Ag. Qualitative estimates can however be easily made based on the observed plasmon resonance band.

Some of the features of plasmon bands and their dependence on the dielectric constant of the medium and the number of free electrons present in the nanocrystals find interesting uses. It is possible to probe events occurring in the vicinity of nanoparticles using the plasmon resonance band. There have been many experiments to demonstrate the high sensitivity of the plasmon band to small changes in the surrounding dielectric. Events that alter the surrounding dielectric such as binding of molecules and the solvent refractive index have been studied using plasmon resonance spectroscopy [66, 76, 77]. Chemisorption of molecules on the surface of the nanocrystals alters the number of free electrons as well as the dielectric constant of the medium, thereby leading to striking changes in the plasmon band [68].

In the case of semiconductor and other particles, the number of free electrons is much smaller and the plasmon absorption band is shifted to the infrared region. The absorption of visible radiation by semiconductor nanocrystals is due to excitonic transitions. Much of our understanding of the absorption processes in semiconductor nanocrystals in the visible region stems from the work of Efros and Brus and coworker [78–80]. They propose a theory based on effective mass approximation to explain the size-dependent changes in the absorption spectra of semiconducting nanocrystals. The absorption spectra can be understood by following the changes in the

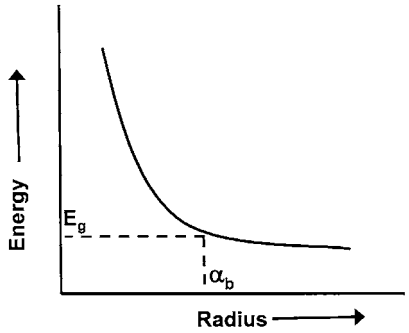

Fig. 1.17. A schematic illustration of the variation of absorption onset vs. the particle diameter. The absorption onset is directly related to the bandgap (E_g) and is constant (bulk like) till the nanocrystal diameter is larger than the exciton diameter, α_b

size of the nanocrystals in comparison to the exciton diameter. It may be recalled that excitons are imaginary quasiparticles produced by pairing of an electron (from the conduction band) and a hole (from the valence band), due to Coulomb interaction. Excitons in semiconductors form hydrogen atom like states with diameters significantly larger than the unit cell length. The exciton diameter is, α_b, given by,

$$\alpha_b = \frac{h^2\epsilon}{e^2}\left[\frac{1}{m_e^*} + \frac{1}{m_h^*}\right], \tag{1.22}$$

where m_h^* is the effective mass of a hole. When the diameter of a nanocrystals, D, is much larger than α_b, the absorption spectrum is similar to that of the bulk. However, when α_b and D become closer, a sharp, size-dependent rise in the absorption onset accompanied by a blue-shift of the absorption maximum is seen. This is schematically illustrated in Fig. 1.17. Thus, CdS, a yellow solid, exhibits an excitonic absorption around 600 nm, which gradually shifts into the UV region as the nanocrystal is decreased till a value below 10 nm. In contrast to metal nanocrystals, the absorption band can be varied over a wide range by changing the dimensions of semiconductor nanocrystals. The excitonic nature of the absorption band permits a direct correlation of the bandgap of the semiconductor nanocrystal with the absorption edge. It is possible to model key effects such as the surface structure and coupling of the electronic states and reproduce the experimental observations [81,82]. However, our understanding of the optical properties is far from being complete.

In addition to properties associated with optical absorption, semiconductor nanocrystals exhibit interesting luminescent behavior. The luminescence is generally dependent on the size of the nanocrystal and the surface structure [83]. A photograph showing changes in the emission wavelength as a function of size of semiconductor quantum dots is shown in Fig. 1.18. The

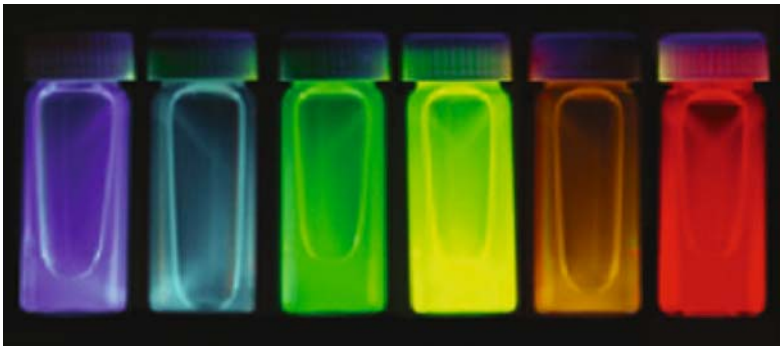

Fig. 1.18. Emission from ZnS coated CdSe nanocrystals of different sizes, dispersed in hexane (reproduced with permission from [83])

surface of a semiconductor nanocrystal can be quite different from that of the metal nanocrystals. Given the directional nature of the covalent bonds present in semiconductors, the surface structure cannot be described by schemes such as the ones indicated in (1.1). Growth defects tend to get concentrated at the surface, leading to surface states with energies in the midgap region, interfering with the emission process. It is, however, possible to obtain highly luminescent semiconductor nanocrystals by careful synthesis. A wide range of applications have been envisaged for luminescent nanocrystals.

1.2.5 Other Properties

An increase in the surface area per unit mass is a direct consequence of reduced dimensions of nanocrystals. The increase in specific surface area assumes significance in catalysis. Heterogenous catalysis benefits from the increase in the number of active sites accompanying the increase in surface area. Thus, nanoscale materials can be useful as powerful catalysts. Further, changes in the electronic structure brought about by quantum confinement effects could be used to tailor the reactivity of nanocrystals. Reactions with no parallels in bulk matter can be carried out through the aid of nanocrystals. A few such reactions have indeed been realized.